The production of triton and reconstruction of 3ΛH with the Heavy Flavor Tracker in Au+Au collisions at STAR

doi: 10.1016/j.nuclphysa.2018.10.023

Available online at www.sciencedirect.com

ScienceDirect

Nuclear Physics A 982 (2019) 811–814

www.elsevier.com/locate/nuclphysa

XXVIIth International Conference on Ultrarelativistic Nucleus-Nucleus Collisions (Quark Matter 2018)

The production of triton and reconstruction of ${}^{3}_{\Lambda}$H with the Heavy Flavor Tracker in Au+Au collisions at STAR

Peng Liu (for the STAR Collaboration)[a,b,c]

[a] *Shanghai Institute of Applied Physics, Chinese Academy of Sciences, Shanghai 201800, China*
[b] *University of Chinese Academy of Sciences, Beijing 100049, China*
[c] *Brookhaven National Laboratory, Upton, New York 11973, USA*

Abstract

The transverse momentum spectra of triton with STAR Beam Energy Scan data from Au+Au collisions at $\sqrt{s_{NN}}$ = 7.7, 11.5, 14.5, 19.6, 27, 39, 62.4, 200 GeV in the centrality classes 0 – 10%, 10 – 20%, 20 – 40% and 40 – 80% are reported. The centrality dependence of the coalescence parameter B_3 of triton and the collision energy dependence of the relative neutron density fluctuation are then calculated. The results indicate that the B_3 decreases from peripheral to central collisions and the neutron density fluctuation shows a non-monotonic collision energy dependence with a peak around collision energy of 20-30 GeV. In addition, we report details about the reconstruction method of ${}^{3}_{\Lambda}$H via ${}^{3}_{\Lambda}\mathrm{H} \rightarrow {}^{3}\mathrm{He} + \pi^-$ and ${}^{3}_{\Lambda}\mathrm{H} \rightarrow \mathrm{d} + \mathrm{p} + \pi^-$ using high statistics data in Au+Au collisions at $\sqrt{s_{NN}}$ = 200 GeV collected in 2014 and 2016 with the Heavy Flavor Tracker.

Keywords: Triton, Neutron density fluctuation, Hypertriton, Mass

1. Introduction

Nucleus-nucleus collisions or the fixed target experiments at the collision energy from a few GeV to the Large Hadron Collider (LHC) energy regime produce abundant light nuclei, strange baryons and their corresponding anti-particles, and even hypernuclei or anti-hypernuclei (hypernuclei are nuclei containing at least one strange baryon) [1–6]. Such collisions provide us an ideal place to study the production of light nuclei and the properties of light hypernuclei.

The production of light nuclei in relativistic heavy-ion collisions is an excellent tool to explore the QCD phase structure and to search for the QCD critical point [7–9]. Light nuclei production in relativistic heavy-ion collisions is described by coalescence [10] and thermodynamic [7, 11–13] models. In a coalescence picture, the invariant yields dN/dp of light nuclei with charge Z and atomic mass number A are denoted as [10]:

$$\mathrm{E_A}\frac{\mathrm{d}^3\mathrm{N_A}}{\mathrm{dp_A^3}} = \mathrm{B_A}\left(\mathrm{E_p}\frac{\mathrm{d}^3\mathrm{N_p}}{\mathrm{dp_p^3}}\right)^{\mathrm{Z}}\left(\mathrm{E_n}\frac{\mathrm{d}^3\mathrm{N_n}}{\mathrm{dp_n^3}}\right)^{\mathrm{A-Z}} \approx \mathrm{B_A}\left(\mathrm{E_p}\frac{\mathrm{d}^3\mathrm{N_p}}{\mathrm{dp_p^3}}\right)^{\mathrm{A}} \quad (1)$$

https://doi.org/10.1016/j.nuclphysa.2018.10.023
0375-9474/

where $p_A = Ap_p$, p_A is the momentum of the cluster and p_p is the momentum of the nucleon in the cluster. The coalescence parameter B_A reflects the probability of nucleon coalescence, which is related to the local nucleon density. In a thermodynamic approach, the effective volume of the nuclear matter at the time of nucleons condensation into nuclear clusters [7], is related to the coalescence parameter B_A:

$$B_A \propto V_{\rm eff}^{1-A} \tag{2}$$

The relative density fluctuation of neutrons ($\Delta n = \langle(\delta n)^2\rangle/\langle n\rangle^2$) at kinetic freeze-out in relativistic heavy-ion collisions is encoded in the yield ratio of light nuclei. This ratio is expressed as [9]:

$$O_{p-d-t} = \frac{N_{^3H} N_p}{N_d^2} \approx g(1 + \Delta n) \tag{3}$$

with $g = 0.29$. Δn is a dimensionless quantity that characterizes the relative density fluctuation of neutrons which is sensitive to the QCD phase transition [9].

The hyperon-nucleon (YN) interaction is of great importance for the understanding of strong interaction and the structure of neutron star [14, 15]. However, our current understanding of YN interaction is poor because of the difficulty in obtaining stable hyperon beams. Hypernuclei are natural hyperon-baryon correlation systems and thus can be used for studying YN interaction through its properties (for example the lifetime and mass). Because of the high spatial resolution of the Heavy Flavor Tracker (HFT) [16] in STAR and the high statistics experiment data collected by STAR at the Relativistic Heavy Ion Collider (RHIC), abundant ${}^3_\Lambda$H are reconstructed with excellent signal/background ratio which allow us to precisely measure the mass of ${}^3_\Lambda$H.

2. Analysis details of triton and ${}^3_\Lambda$H

In this analysis, the triton is identified by the combined usage of the Time Projection Chamber (TPC) and the Time Of Flight (TOF) detectors. The energy loss, the acceptance and the efficiency of triton in the detector are corrected by using the STAR embedding data and the corrections are derived from a Monte Carlo GEANT3 simulation with STAR detector geometry [17]. The ${}^3_\Lambda$H is reconstructed through its 2-body and 3-body decay channels ${}^3_\Lambda\mathrm{H} \rightarrow {}^3\mathrm{He} + \pi^-$ and ${}^3_\Lambda\mathrm{H} \rightarrow \mathrm{d} + \mathrm{p} + \pi^-$ with data collected in 2014 (about 1.2 billion minimum-bias triggered events) and in 2016 (about 3.4 billion minimum-bias triggered events) by STAR with HFT in Au+Au collisions at $\sqrt{s_{NN}} = 200\,\mathrm{GeV}$. The HFT detector consists of three subsystems, pixel detector (PXL), intermediate silicon tracker (IST) and silicon strip detector (SSD). Because of the high spatial resolution of HFT [16], the reconstructed tracks of all decay daughters are required to have at least three hits in HFT (at least 2 hits in PXL and 1 hit in IST). In the reconstruction of 3-body decay, the identification for the decay daughters is performed by combining the PID information obtained from TPC and TOF. In the reconstruction of 2-body decay, TPC is used for identifying the decay daughters. The reconstructed invariant mass can be expressed as:

$$M^2 = \left(\sum E_i\right)^2 - \left(\sum \vec{p}_i\right)^2 \tag{4}$$

where M represents the mother's mass (also known as invariant mass). $E_i = \sqrt{m_i^2 + \vec{p}_i^2}$ represents the total energy of i-th daughter. m_i and $\vec{p}_i$ are the rest mass and momentum of i-th daughter, respectively. In our analysis, the masses of ^{3}He and d are taken from CODATA [18] and the masses of p and π^- are taken from PDG [19]. The momentum of decay daughters are corrected by means of a dedicated simulation, taking into account the STAR HFT geometry to estimate the charged particles energy loss in the material in front of and in the TPC. The reconstructed invariant mass distributions are shown in Fig. 1. In Fig. 1, the red curves represent the fit function using a Gaussian with a linear polynomial function. Comparing with previous STAR results [2], invariant mass distributions shown in Fig. 1 feature high signal/background properties. Therefore, precise measurement on the mass and lifetime of ${}^3_\Lambda$H can be done through these new data.

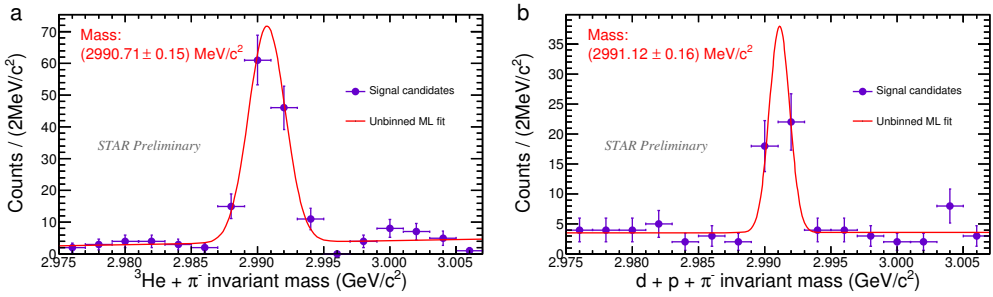

Fig. 1: The invariant mass distributions of ${}^{3}_{\Lambda}\mathrm{H}$ reconstructed through 2-body (panel a) and 3-body (panel b) decay channels with the experimental data collected by the STAR detector in 2014 and 2016. The red curves show the fit function using a Gaussian with a linear polynomial function.

3. The production of triton

Measurements on the triton are based on the RHIC Beam Energy Scan (BES) data from Au+Au collisions at $\sqrt{s_{NN}}$ = 7.7, 11.5, 14.5, 19.6, 27, 39, 62.4, 200 GeV at midrapidity ($|y| < 0.5$) with the STAR TPC and TOF detectors. The transverse momentum spectra of identified triton in the centrality classes 0 – 10%, 10 – 20%, 20 – 40% and 40 – 80% are shown in Fig. 2. The spectra show a hardening with increasing centrality and are fitted with individual blast-wave functions.

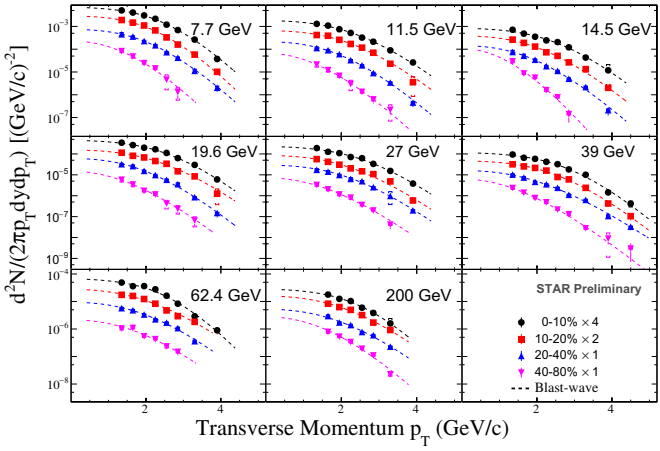

Fig. 2: Midrapidity ($|y| < 0.5$) transverse momentum spectra for triton in Au+Au collisions at $\sqrt{s_{NN}}$ = 7.7, 11.5, 14.5, 19.6, 27, 39, 62.4 and 200 GeV in the centrality classes 0 – 10%, 10 – 20%, 20 – 40% and 40 – 80%. The dashed lines are the individual fits to the data with blast-wave functions. The box shows the systematic uncertainty and the vertical line shows the statistical uncertainty.

According to Eq. 1, the coalescence parameter B_3^t can be calculated through the transverse momentum spectra of triton and proton [20]. The coalescence parameter B_3^t as a function of p_T/A for triton in Au+Au collisions at $\sqrt{s_{NN}}$ = 7.7 GeV and 200 GeV in the centrality classes 0 – 10%, 10 – 20%, 20 – 40% and 40 – 80% is shown in the left panel and middle panel of Fig. 3. B_3^t decreases from peripheral to central collisions which means the freeze-out volume increases from peripheral to central collisions based on thermodynamic picture. From the triton transverse momentum spectra we can also extract the yield of triton. Therefore, the neutron density fluctuation can be calculated through the Eq. 3 with the deuteron yield [21] and proton yield [20]. The neutron density fluctuation Δn in the right panel of Fig. 3 shows a non-monotonic energy dependence with a peak around collision energy 20-30 GeV which indicates the relative neutron density

fluctuations become the largest in Au+Au collisions in this energy range. The details of this analysis can be found in [22].

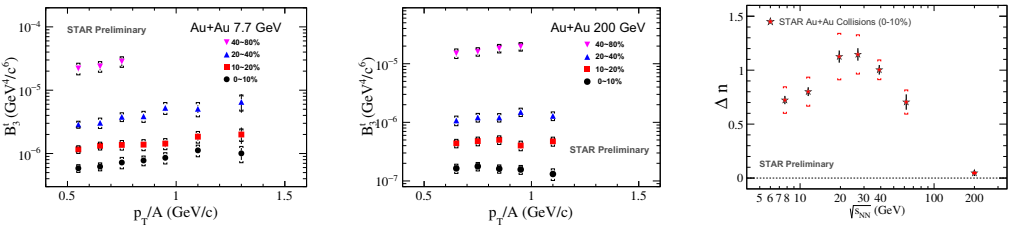

Fig. 3: (Left and middle panels) Coalescence parameter B_3^t as a function of p_T/A for triton in Au+Au collisions at $\sqrt{s_{NN}}$ = 7.7 GeV and 200 GeV in the centrality classes 0 – 10%, 10 – 20%, 20 – 40% and 40 – 80%. The vertical line is the statistical uncertainty and the bracket is the systematic uncertainty. (Right panel) The collision energy dependence of relative neutron density fluctuation Δn in Au+Au most central collisions. The vertical line is the statistical uncertainty and the bracket is the systematic uncertainty.

4. Conclusions

We report the transverse momentum spectra of triton obtained by analyzing the STAR Beam Energy Scan data from Au+Au collisions at $\sqrt{s_{NN}}$ = 7.7, 11.5, 14.5, 19.6, 27, 39, 62.4, 200 GeV in the centrality classes 0 – 10%, 10 – 20%, 20 – 40% and 40 – 80%. We find that the B_3^t decreases from peripheral to central collisions and the neutron density fluctuation shows a non-monotonic collision energy dependence with a peak around a collision energy of 20-30 GeV. We also report the details on the reconstruction of ${}^3_\Lambda$H and the reconstructed signals of ${}^3_\Lambda$H will be used for measuring the ${}^3_\Lambda$H mass and lifetime with improved precision.

5. Acknowledgements

This work was supported in part by the Major State Basic Research Development Program in China under Contract No. 2014CB845401, the National Natural Science Foundation of China under contract Nos. 11775288, 11421505 and 11520101004, the China Scholarship Council under contract No. 201704910615.

References

[1] Abelev, B.I. et al. (STAR Collaboration). *Science* **328**, 58 (2010).
[2] Adamczyk, L. et al. (STAR Collaboration). *Phys. Rev. C* **97**, 054909 (2018).
[3] Armstrong, T. et al. (E864 Collaboration). *Phys. Rev. Lett.* **83**, 5431 (1999).
[4] Liu, P., Chen, J.-H., Ma, Y.-G. and Zhang, S. *Nucl. Sci. Tech.* **28**, 55 (2017).
[5] Lea, R. (For the ALICE Collaboration). *Nucl. Phys. A* **914**, 415 (2013).
[6] Chen, J., Keane, D., Ma, Y.-G., Tang, A. and Xu, Z. *Phys. Rep.* (2018). URL `https://doi.org/10.1016/j.physrep.2018.07.002 (in press)`.
[7] Mekjian, A. Z. *Phys. Rev. C* **17**, 1051 (1978).
[8] Zhang, S. *et al. Phys. Lett. B* **684**, 224 (2010).
[9] Sun, K.-J., Chen, L.-W., Ko, C. M. and Xu, Z. *Phys. Lett. B* **774**, 103 (2017).
[10] Csernai, L. and Kapusta, J. I. *Phys. Rep.* **131**, 223 (1986).
[11] Andronic, A., Braun-Munzinger, P., Stachel, J. and Stöcker, H. *Phys. Lett. B* **697**, 203 (2011).
[12] Cleymans, J. *et al. Phys. Rev. C* **84**, 054916 (2011).
[13] Andronic, A., Braun-Munzinger, P., Redlich, K. and Stachel, J. *J. Phys. G* **38**, 124081 (2011).
[14] Lattimer, J. M. and Prakash, M. *Science* **304**, 536 (2004).
[15] Schaffner-Bielich, J. *Nucl. Phys. A* **804**, 309 (2008).
[16] Qiu, H. (For the STAR Collaboration). *Nucl. Phys. A* **931**, 1141 (2014).
[17] Fine, V., Fisyak, Y., Victor, P. and Wenaus, T. *Comput. Phys. Commun.* **140**, 76 (2001).
[18] Mohr, P. J., Newell, D. B. and Taylor, B. N. *Rev. Mod. Phys.* **88**, 035009 (2016).
[19] Tanabashi, M. et al. (Particle Data Group). *Phys. Rev. D* **98**, 030001 (2018).
[20] Adamczyk, L. et al. (STAR Collaboration). arXiv:1707.01988v1 [nucl-ex] .
[21] Yu, N. (For the STAR Collaboration). *Nucl. Phys. A* **967**, 788 (2017).
[22] Zhang, D. (For the STAR Collaboration). Quark Matter 2018 Poster ID: 450.